Electronic Supplementary Information

Comparing electrocatalytic and chemical oxygen reduction reaction by a molecular copper complex

Lesa Dutta,[a] Avijit Das,[b] Babar Hasan,[a] Sayantan Paria,*[b] and Dhrubajyoti Mondal*[a]

[a] Department of Chemistry, Visva-Bharati (A Central University), Santiniketan 731235, West Bengal, India, E-mail: (dhrubajyoti.mondal@visva-bharati.ac.in and dhruba.iitd@gmail.com)

[b] Department of Chemistry, Indian Institute of Technology (IIT) Delhi, Hauz Khas, New Delhi 110016, India; Email: sparia@chemistry.iitd.ac.in

Experimental section

Materials.

The ligand *N*-(3-benzyl-5-chloro-2-hydroxybenzyl)-*N,N*-bis(2-pyridylmethyl)-amine (HL_1) was prepared by Mannich-type condensation reaction according to the previously reported method.[1] Dipicolylamine, paraformaldehyde, 2-benzyl-4-chlorophenol, trifluoroacetic acid, and deuterated solvents were purchased from Sigma-Aldrich. All other compounds were acquired from Merck-India and utilized without additional purification. The solvents were reagent grade, dried by standard procedure,[2] and distilled under a nitrogen atmosphere prior to their use.

Physical Measurements.

FTIR spectra of the samples were measured on a Shimadzu IRAffinity-1S FTIR spectrophotometer in the ATR mode. UV-vis spectra of the Cu complexes were recorded in a Shimadzu-3100 UV/Vis-NIR spectrophotometer and an Agilent 8454 Spectrometer. Elemental analyses (for C, H, and N) were performed at IACS on a PerkinElmer model 2400 Series II CHNS Analyzer. Mass spectrometry data of the ligand and Cu complexes were performed with a Waters Xevo G2-XSQT mass spectrometer. ^{1}H NMR spectra were measured at room temperature with a Bruker Advance (400 MHz) spectrometer using $SiMe_4$ as an internal reference. Deuterated chloroform ($CDCl_3$) was used as a solvent. EPR spectra of the Cu(II) complexes were recorded in a Bruker EPR spectrometer (Biospin, EMXmicro A200) at 77K using a liquid N_2 Dewar Flask.

Cyclic voltammetry (CV) was recorded in acetone solution on a CH Instruments (CHI600F electrochemical analyzer) using a glassy carbon disk working and a platinum wire counter electrode. An Ag/AgCl (3 M aqueous KCl) electrode was used for reference, and the Fc/Fc^+ couple as the internal standard. Solutions were ~0.5 mM in samples and contained 0.1 M TBAP (Tetrabutylammonium hexafluorophosphate) as a supporting electrolyte.

Rotating Ring Disk Electrode (RRDE) instrument. The Rotating Ring-Disk Electrode (RRDE) experiment was conducted using a Metrohm Autolab potentiostat. The working electrode comprised a glassy carbon disk (5 mm in diameter) and a platinum ring (0.1 cm^2). A platinum wire was used as the counter electrode, while an Ag/AgCl electrode in saturated KCl was employed as the reference electrode. The RRDE measurement was performed in an O_2-saturated acetone solution (50 mM ^{n}Bu_4NPF_6) containing Cu complexes (0.5 mM) and 10 mM trifluoroacetic acid (TFAH). Linear sweep voltammetry (LSV) data were recorded at varying rotation rates (200–1000 rpm). The percentage yield of H_2O_2 and the number of electrons (n) involved in the oxygen reduction reaction (ORR) were determined using equations S1 and S2.

$$\%\ H_2O_2 = \frac{2 \times \frac{i_{ring}}{N}}{i_{disk} + \frac{i_{ring}}{N}} \times 100 \qquad \text{(S1)}$$

$$n = \frac{4 \times i_{disk}}{i_{disk} + \frac{i_{ring}}{N}} \qquad \text{(S2)}$$

Where N is the collection efficiency of the electrode, i_{ring} and i_{disk} are the values of ring and disk current, respectively.

Kinetic Isotope Effect. To elucidate the influence of protons in the oxygen reduction reaction (ORR), the kinetic isotope effect (KIE) was investigated using deuterated trifluoroacetic acid (TFA-d) as the proton source.

Chemical kinetics Data analysis. Kinetic analyses were performed using an Agilent 8454 diode array spectrophotometer equipped with a UNISOKU cryostat (Japan), which allows temperature control of the reaction solution within the range of −80 to 100 °C. The catalytic oxygen reduction reaction (ORR) in the presence of **1** was carried out at 25 °C in a 1 cm pathlength cuvette using acetone as the solvent. The catalytic experiments were conducted with a catalytic amount of **1** in the presence of excess decamethylferrocene (Fc*), trifluoroacetic acid (TFAH), and molecular oxygen (O_2) in acetone. The reaction progress was monitored at 780 nm in the UV-vis spectrum, corresponding to the formation of the decamethylferrocene cation (Fc^{*+}). The dependence of the catalytic rate law on the concentration of each substrate (**1**, TFAH, O_2, and Fc*) was determined by varying the concentration of a single substrate while maintaining the concentrations of the others constant. Variations in the concentrations of the **1**, TFAH, and Fc* were conducted in an O_2-saturated acetone solution. The pseudo-first-order rate constant (k_{obs}) for each reaction was obtained from the slope of a plot of ln(ΔA) versus time, while the second-order rate constant (k_2) was determined from the slope of a plot of k_{obs} versus substrate concentration.

Product Selectivity Check during Chemical ORR. The oxygen reduction reaction (ORR) was monitored using UV-vis spectroscopy. Upon saturation of the time trace at 780 nm, an aliquot of 100 μL of the reaction solution was withdrawn and subsequently diluted with 5 mL of distilled water and 10 mL of dichloromethane (DCM). A 3 mL portion of the aqueous phase was transferred to a cuvette, followed by the addition of 100 μL of a 0.1 M solution of $Ti(O)SO_4$. The reaction mixture was then analysed at 405 nm using UV-vis spectroscopy. No significant change in absorbance at 405 nm was observed under these conditions suggesting H_2O is a significant product.

X-ray Crystallography

Suitable crystals of **1** (brown block, 0.12 × 0.12 × 0.1mm^3) and **2** (blue block, 0.2 × 0.18 × 0.16 mm^3) were mounted on glass fibers coated with perfluoropolyether oil before mounting. Intensity data for the aligned crystals were measured employing a Bruker SMART APEX II CCD diffractometer equipped with a monochromatized Mo K_α radiation (λ = 0.71073 Å) source at 293(2) K. No crystal decay was observed during the data collection. In all cases, absorption corrections based on multiscans using the SADABS software[3] were applied. The structures were solved by direct methods[4] and refined on F^2 by a full-matrix least-squares procedure based on all data minimizing $wR = [\sum[w(F_0^2 - F_c^2)^2] / \sum(F_0^2)^2]^{½}$, $R = \sum | |F_0| - |F_c| | / \sum|F_0|$, and $S = [\sum[w(F_0^2 - F_c^2)^2] / (n - p)]^{½}$. The structures were solved using Olex2.solve 1.5 and refined with SHELXL2019.[5] All non-hydrogen atoms were refined anisotropically. The hydrogen atoms were calculated and isotropically fixed in the final refinement [d(C-H) = 0.95 Å, with the isotropic thermal parameter of $U_{iso}(H) = 1.2\ U_{iso}(C)$]. The SMART and SAINT software packages[6] were used for data collection and reduction, respectively. The geometry of the disordered ClO_4^- anion was modelled using the Idealized Molecular Geometry Library. Crystallographic data of Cu complexes are given in Table S1, and bond parameters are mentioned in Table S2−S3.

Table S1. Summary of the Crystallographic Data for the Complex **1** and **2**.

Parameters	**1**	**2**
Empirical formula	$C_{26}H_{25}Cl_2CuN_3O_6$	$C_{52}H_{51}N_6O_{22}Cl_6Cu_2$

Formula weight	609.93	1451.77
Temperature/K	293(2)	293.15
Crystal system	triclinic	monoclinic
Space group	P-1	Cc
a/Å	9.1916(8)	12.8921(13)
b/Å	11.5805(10)	16.3316(17)
c/Å	13.7720(12)	29.441(3)
α/°	70.993(2)	90
β/°	85.658(2)	96.406(2)
γ/°	72.744(2)	90
Volume/Å^3	1323.3(2)	6160.1(11)
Z	2	4
ρ_{calc}g/cm^3	1.531	1.565
μ/mm^{-1}	1.074	1.032
F(000)	626.0	2964
Crystal size/mm^3	0.12 × 0.12 × 0.1	0.2 × 0.18 × 0.16
Radiation	MoKα (λ = 0.71073)	MoKα (λ = 0.71073)
2Θ range for data collection/°	3.128 to 64.114	2.784 to 48.666
Index ranges	-13 ≤ h ≤ 13, -17 ≤ k ≤ 16, -19 ≤ l ≤ 17	-14 ≤ h ≤ 14, -18 ≤ k ≤ 18, -34 ≤ l ≤ 34
Reflections collected	19625	26747
Independent reflections	7634 [R_{int} = 0.0254, R_{sigma} = 0.0347]	9654 [R_{int} = 0.0386, R_{sigma} = 0.0495]
Data/restraints/parameters	7634/1/351	9654/153/801
Goodness-of-fit on F^2	1.077	1.016
Final R indexes [I>=2σ (I)]	R_1 = 0.0466, wR_2 = 0.1141	R_1 = 0.0480, wR_2 = 0.1230
Final R indexes [all data]	R_1 = 0.0679, wR_2 = 0.1277	R_1 = 0.0574, wR_2 = 0.1305
Largest diff. peak/hole / e Å^{-3}	0.69/-0.81	0.56/-0.31

$^a R = \sum||F_o| - |F_c||/\sum|F_o|$. $^b wR = [\sum[w((F_o^2 - F_c^2)^2]/\sum w(F_o^2)^2]^{1/2}$

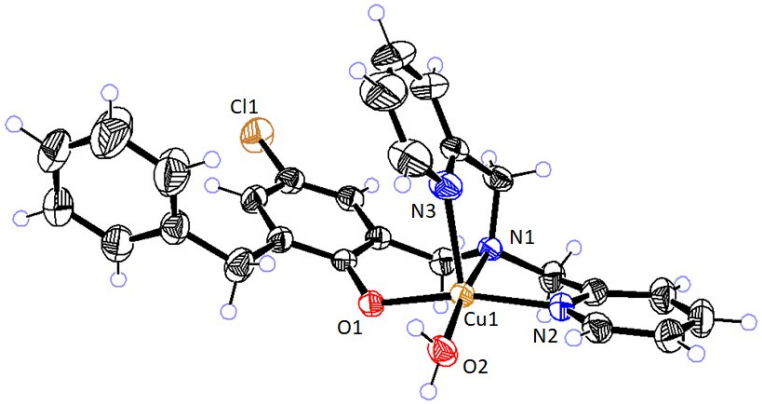

Table S2. Selected Bond Angles and Distances in complex **1**.

Bond Length/Å	Bond Angle/°

Cu1-O1	1.9222(16)	O1-Cu1-O2	89.40(8)
Cu1-O2	1.9961(18)	O1-Cu1-N2	164.13(8)
Cu1-N2	1.986(2)	O1-Cu1-N1	94.95(7)
Cu1-N1	2.0577(19)	O1-Cu1-N3	91.92(9)
Cu1-N3	2.260(2)	O2-Cu1-N1	172.99(8)
		O2-Cu1-N3	104.24(9)
		N2-Cu1-O2	91.88(8)
		N2-Cu1-N1	82.44(8)
		N2-Cu1-N3	103.07(9)
		N1-Cu1-N3	81.15(8)

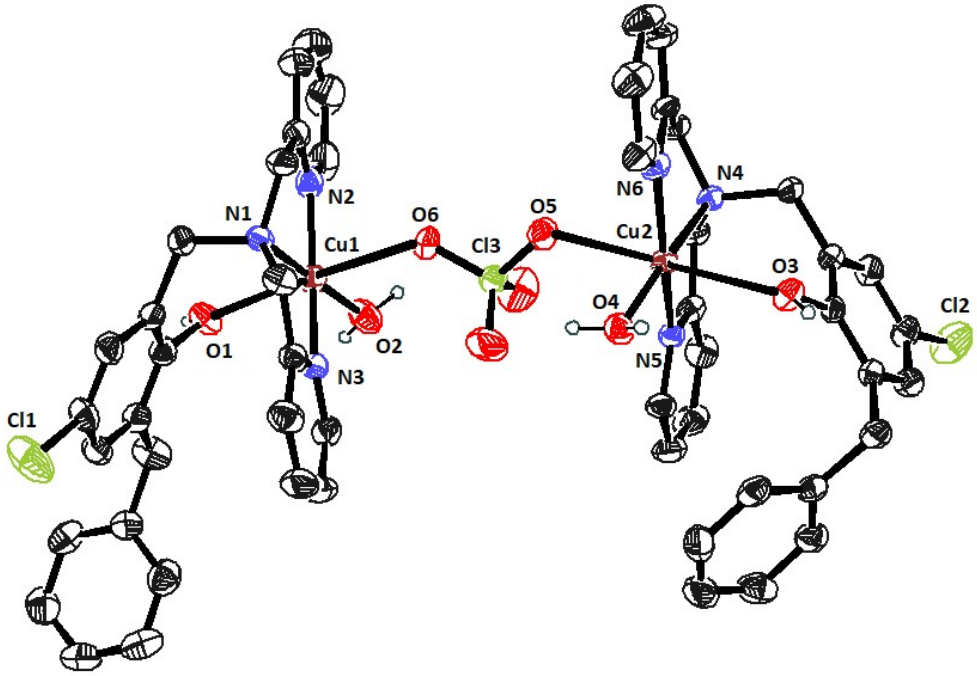

Table S3. Selected Bond Angles and Distances in complex **2**.

Bond Length/Å		Bond Angle/°	
Cu2-N4	1.997(7)	N4-Cu2-O3	103.07(9)
Cu2-N5	1.963(7)	N5-Cu2-N4	103.07(9)
Cu2-O3	2.420(6)	N5-Cu2-O3	103.07(9)
Cu2-N6	1.976(7)	N5-Cu2-N6	103.07(9)
Cu2-O5	2.505(7)	N5-Cu2-O4	103.07(9)
Cu2-O4	1.963(7)	N6-Cu2-N4	103.07(9)
Cu1-N2	1.989(6)	N6-Cu2-O3	103.07(9)
Cu1-N1	2.015(7)	O4-Cu2-N4	103.07(9)
Cu1-N3	1.981(6)	O4-Cu2-O3	103.07(9)
Cu1-O1	2.465(7)	O4-Cu2-N6	103.07(9)
Cu1-O6	2.458(7)	N2-Cu1-N1	103.07(9)
Cu1-O2	1.976(6)	N3-Cu1-N2	103.07(9)
		N3-Cu1-N1	83.1(3)
		O2-Cu1-N2	99.1(3)
		O2-Cu1-N1	177.6(2)

	O2-Cu1-N3	94.9(3)

Experimental Section

Synthesis of ligand

N-(3-benzyl-5-chloro-2-hydroxybenzyl)-N,N-bis(2-pyridylmethyl)-amine (HL_1)
Dipicolylamine (10 mmol, 2.0 g), paraformaldehyde (10 mmol, 0.3 g), and 2-benzyl-4-chlorophenol (10 mmol, 2.18 g) were taken in methanol (30 mL). The solution was heated under reflux for ca. 14 h. It was then cooled to room temperature and rotary evaporated to ca. 15 mL volume, resulting in the formation of a white solid. The solid was filtered and recrystallized from acetonitrile to obtain a white crystalline product. Yield: 70 %. Anal. Calc. for $C_{26}H_{24}N_3OCl$: C, 72.63; H, 5.63; N, 9.77. Found: C, 72.45; H, 5.59; N, 9.75%. FT-IR bands (cm^{-1}): 3045(b), 1591(s), 1475(s), 1433(s), 1369(s), 1228(s), 1000(m), 972(m), 865(m), 757(s), 702(m). ^1H NMR ($CDCl_3$, 400 MHz, ppm): 3.78 (s, 2H), 3.88 (s, 4H), 4.04 (s, 2H), 6.94 (d, 2H), 7.17 (m, 2H), 7.20(m, 7H), 7.62 (t, 2H), 8.58 (d, 2H). ESI-MS (positive) in CH_3CN: *m/z* 430.23, 100 %, $(M + H)^+$.

N-(3-benzyl-5-chloro-2-methoxybenzyl)-N,N-bis(2-pyridylmethyl)-amine (L_2)
HL_1 (1 mmol, 429 mg) was dissolved in dry tetrahydrofuran (THF, 10 mL) under an inert atmosphere and stirred at 0 °C for 1 h. Sodium hydride (60 wt %, 100 mg, 1 mmol) was then added gradually, and the reaction mixture was stirred for an additional 3 h at 0 °C. Afterward, methyl iodide (5 mmol, 0.3 mL) was added dropwise while maintaining the temperature at 0 °C. The reaction mixture was then allowed to warm to room temperature and stirred for 24 h. Upon completion, the reaction was quenched with brine solution and extracted with ethyl acetate (3 × 20 mL). The combined organic layers were dried over anhydrous sodium sulfate, filtered, and concentrated under reduced pressure to afford a highly viscous yellow liquid as a product. Yield: 65 %. ^1H NMR ($CDCl_3$, 400 MHz, ppm): 3.49 (s, 3H), 3.69 (s, 2H), 3.79 (s, 4H), 3.88 (s, 2H), 6.86 (d, 1H), 7.08 (m, 2H), 7.19 (m, 5H), 7.43 (d, 1H), 7.49 (d, 2H), 7.61(t, 2H), 8.45 (d, 2H). ESI-MS (positive) in CH_3CN: *m/z* 444.19, 100 %, $(M + H)^+$.

Preparation of Complexes

Caution! *Perchlorate compounds are potentially explosive. Prepare and handle a tiny amount of material carefully.*

Synthesis of $[(L_1)Cu(H_2O)]ClO_4$ (1)
The ligand HL_1 (0.25 mmol, 107 mg) was dissolved in 25 mL of methanol, followed by the addition of triethylamine (0.25 mmol, 25 mg). The reaction mixture was stirred for 10 minutes. To this was added $Cu(ClO_4)_2 \cdot 6H_2O$ (0.25 mmol, 92 mg). The resulting brown solution was stirred for 2.5 hours. Then, the solution was reduced to approximately 15 mL using a rotary evaporator, filtered through a Celite bed, and kept at 4 °C to allow for slow crystallization. After 5 days, a block-shaped dark brown crystalline product was collected by filtration. Some of these crystals were of diffraction grade and used directly for X-ray crystallographic analysis. Yield: 60 %. Anal. Calcd for $C_{26}H_{25}Cl_2N_3O_6Cu$: C, 51.20; H, 4.13; N, 6.89. Found: C, 51.15; H, 4.09; N, 6.88%. FT-IR bands (cm^{-1}): 3412 (m), 1446 (m), 1612 (m), 1222 (m), 1103 (s),

1053 (s), 622 (s). UV-Vis (MeOH) [λ_{max}, nm (ε, L mol^{-1}cm^{-1})]: 436 (1270), 660 (210), 850 (20). ESI-MS (positive) in CH_3OH: *m/z* 491.08, $[(L_1)Cu]^+$.

Synthesis of $[\{(HL_1)Cu(H_2O)\}_2(ClO_4)](ClO_4)_3\cdot 3H_2O$ (2)

HL_1 (0.25 mmol, 107 mg) and $Cu(ClO_4)_2\cdot 6H_2O$ (0.25 mmol, 92 mg) were dissolved in CH_3OH (25 mL) solvent. A bright blue solution immediately formed, and the solution was allowed to stir for 2.5 hours. The volume of the resulting solution was gradually reduced to approximately 15 mL using a rotary evaporator under reduced pressure. The concentrated mixture was then filtered through a Celite bed to remove any insoluble impurities. The filtrate was left undisturbed at ambient temperature for slow crystallization. After a duration of seven days, block-shaped blue-colored crystals were obtained. Some of these crystals exhibited high-quality diffraction properties and were directly utilized for single-crystal X-ray crystallographic analysis. Yield: 55 %. Anal. Calcd for $C_{52}H_{58}Cl_6N_6O_{23}Cu_2$: C, 42.35; H, 3.96; N, 5.70. Found: C, 42.15; H, 3.91; N, 5.68%. FT-IR bands (cm^{-1}): 3400 (m), 1612 (m), 1443 (m), 1069 (s), 619 (s). UV-Vis (MeOH) [λ_{max}, nm (ε, L mol^{-1}cm^{-1})]: 479 (124), 670 (195). ESI-MS (positive) in CH_3OH: *m/z* 491.08, $[(L_1)Cu]^+$; 593.03, $\{[(L_1H)Cu\text{-}(ClO_4)\text{-}Cu(L_1H)]ClO_4\}^{2+}$

Synthesis of $[(L_2)Cu(H_2O)](ClO_4)_2$ (3)

L_2 (0.25 mmol, 111 mg) and $Cu(ClO_4)_2\cdot 6H_2O$ (0.25 mmol, 93 mg) were dissolved in CH_3OH (20 mL) solvent. A bright green solution immediately formed, and the solution was allowed to stir for 2.5 hours. The volume of the resulting solution was gradually reduced to approximately 10 mL using a rotary evaporator under reduced pressure. The concentrated mixture was then filtered through a Celite bed to remove any insoluble impurities. The filtrate was left undisturbed at ambient temperature for slow evaporation, which produces a green colour complex. Yield: 45 %. UV-Vis (MeOH) [λ_{max}, nm]: 406 (340), 430 (373), 684 (110). ESI-MS (positive) in CH_3CN: m/z 506.11, $[(L_2)Cu]^+$; 523.11, $[(L_2)Cu(OH)]^+$; 605.06 $[(L_2)Cu(ClO_4)]^+$.

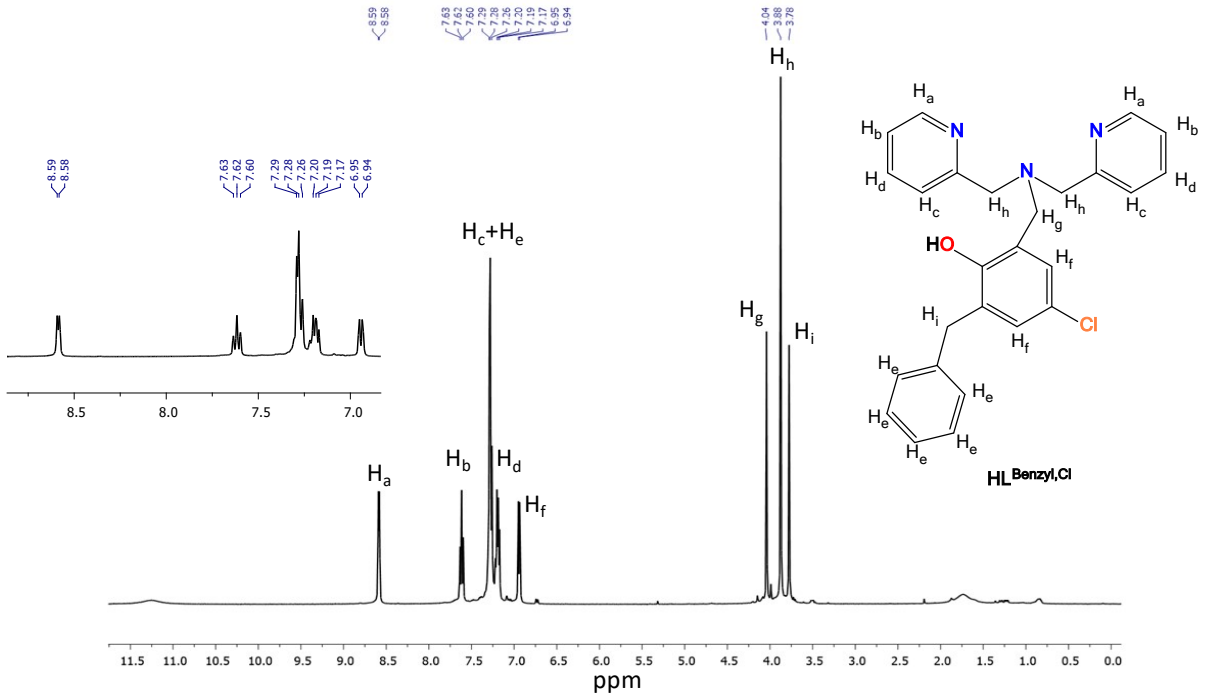

Figure S1. ^{1}H NMR of HL_1 Ligand.

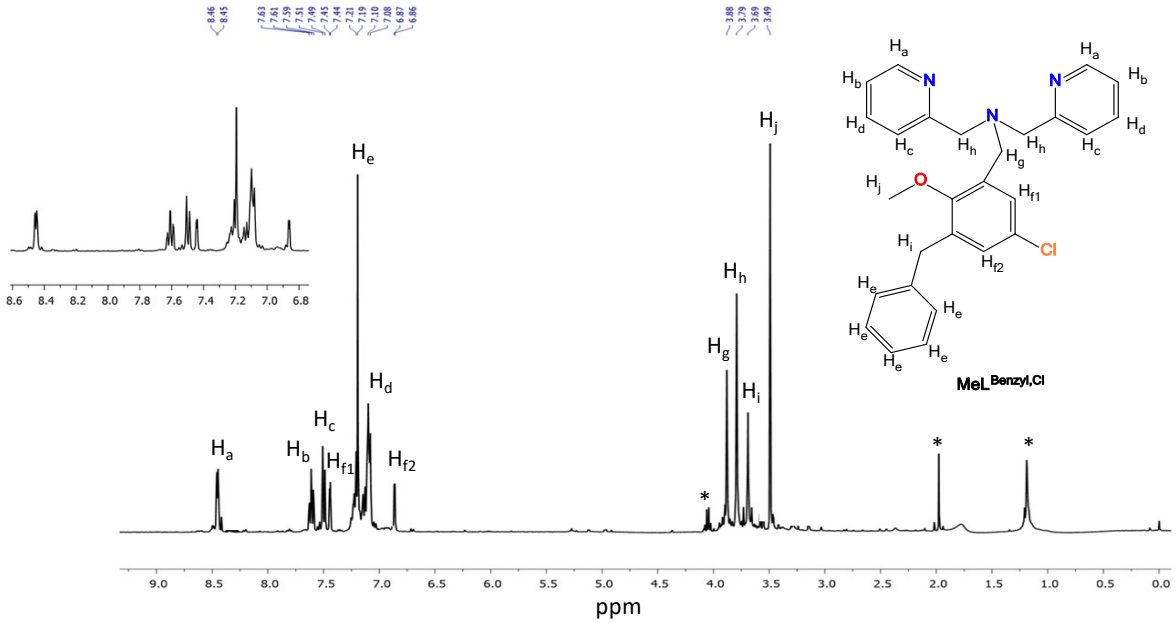

Figure S2. ^{1}H NMR of L_2 Ligand in $CDCl_3$ (* = peak of ethyl acetate).

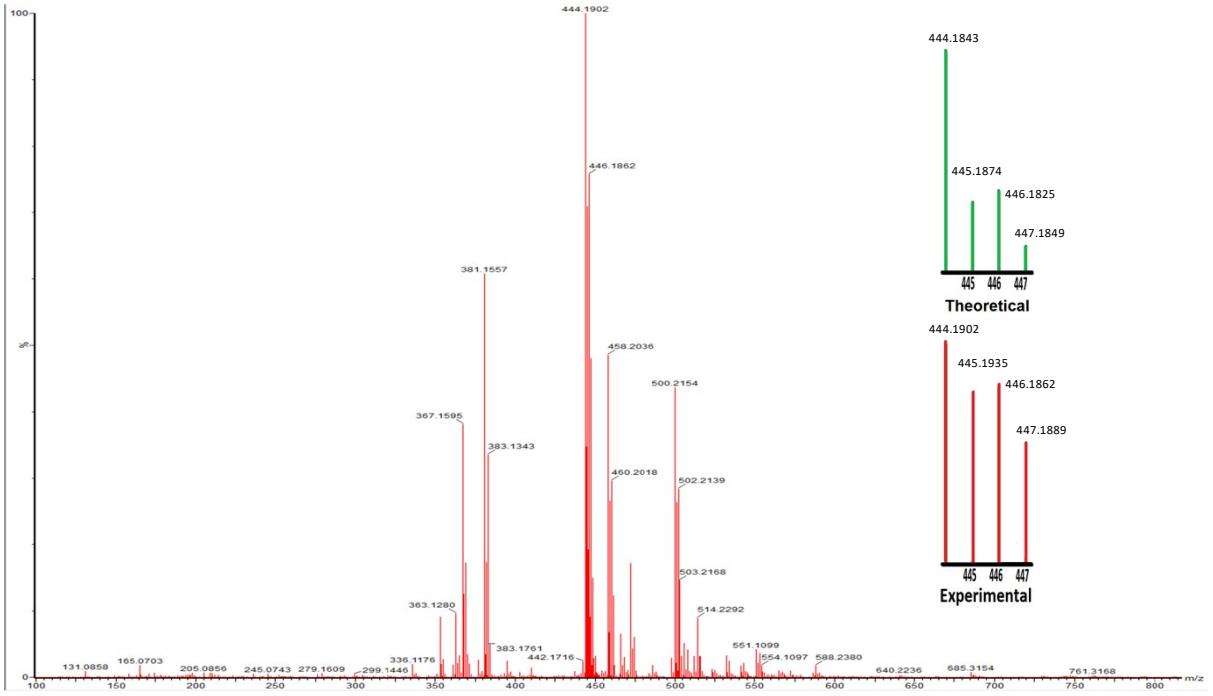

Figure S3. ESI-MS (positive mode) of L_2 in methanol. Calculated *m/z* for $[L_2 + H]^+$: 444.184, Obtained m/z = 444.190.

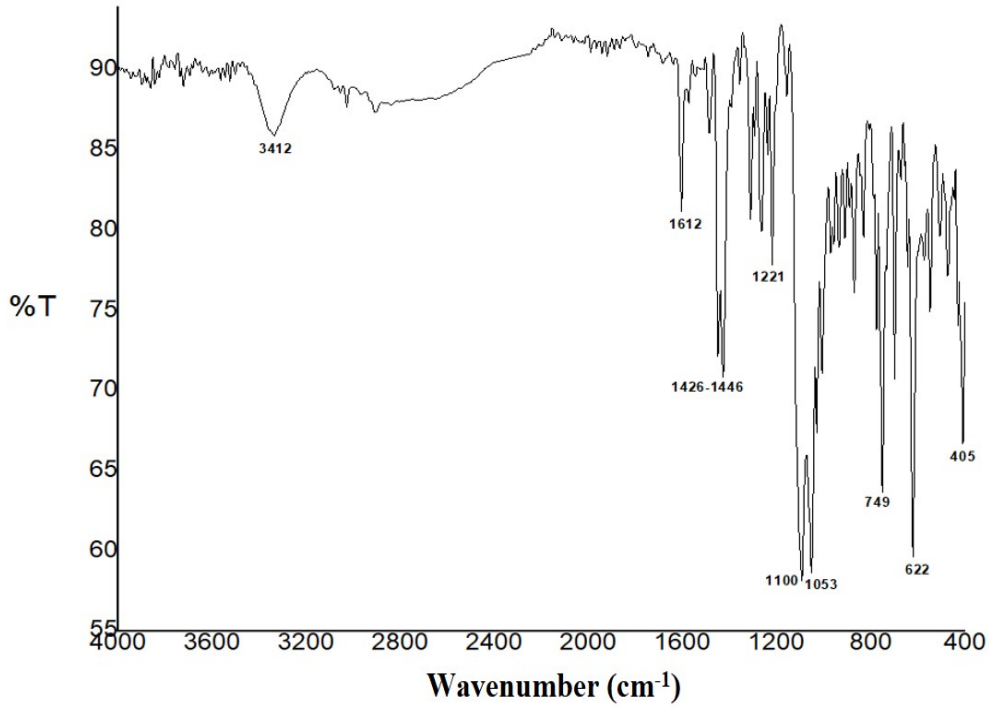

Figure S4. FT-IR spectra of complex **1.**

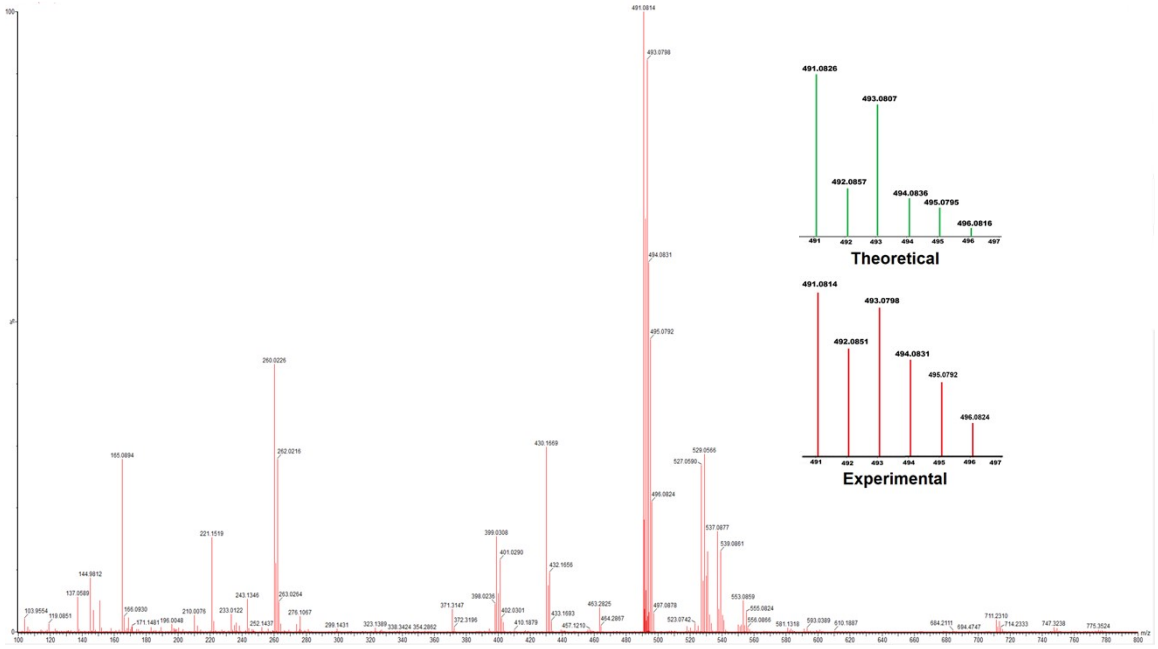

Figure S5. ESI-MS (positive mode) of **1** in methanol. Calculated m/Z for $[(L_1)Cu]^+$: 491.082, Obtained *m/z*: 491.081.

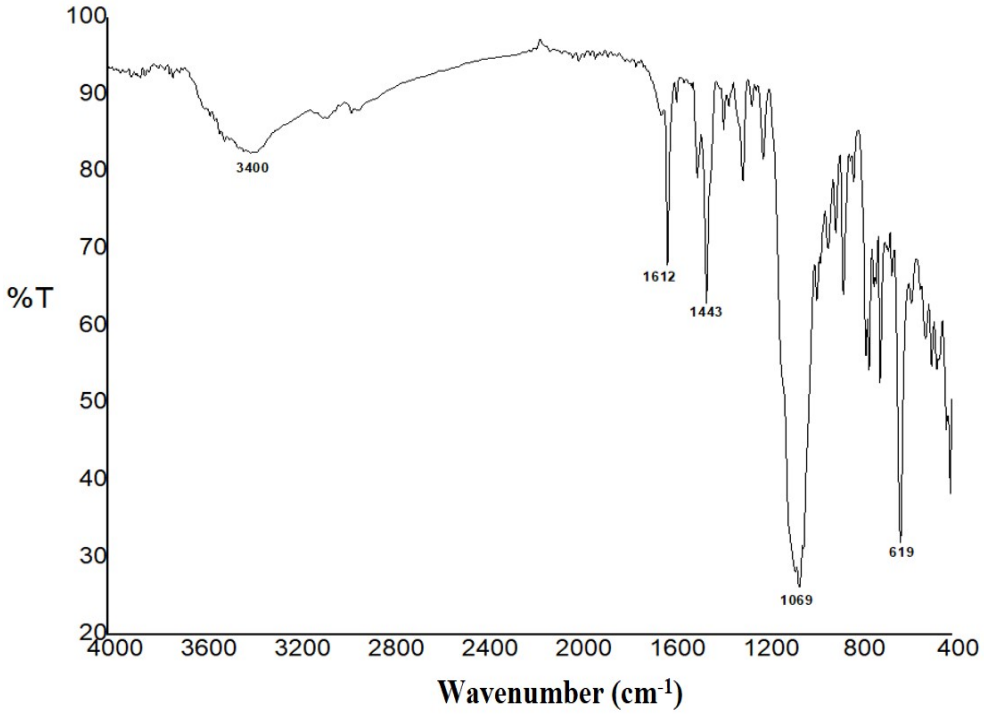

Figure S6. FT-IR spectra of complex **2**.

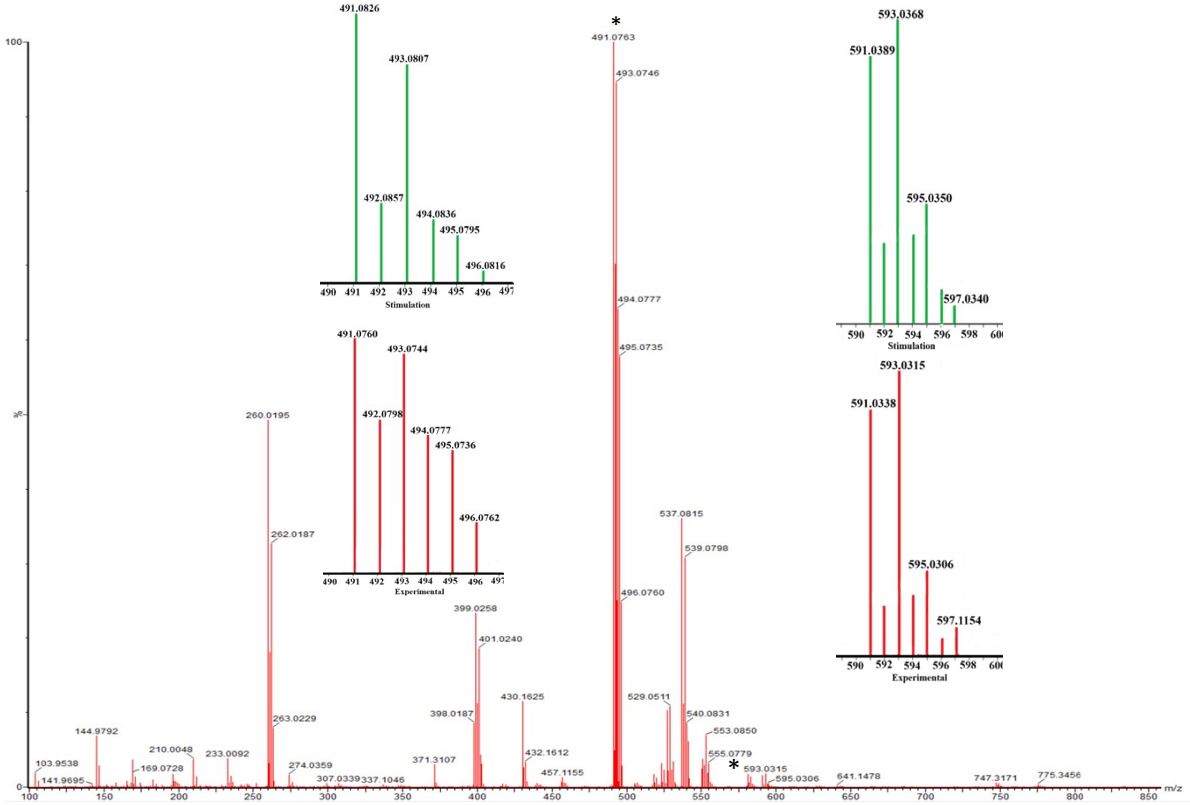

Figure S7. ESI-MS (positive mode) of **2** in methanol. Calculated *m/z* for $[(L_1)Cu]^+$: 491.082, Obtained *m/z*: 491.076; Calculated *m/z* for $\{[(L_1H)Cu\text{-}(ClO_4)\text{-}Cu(L_1H)]ClO_4\}^{2+}$: 593.039, Obtained *m/z*: 593.034.

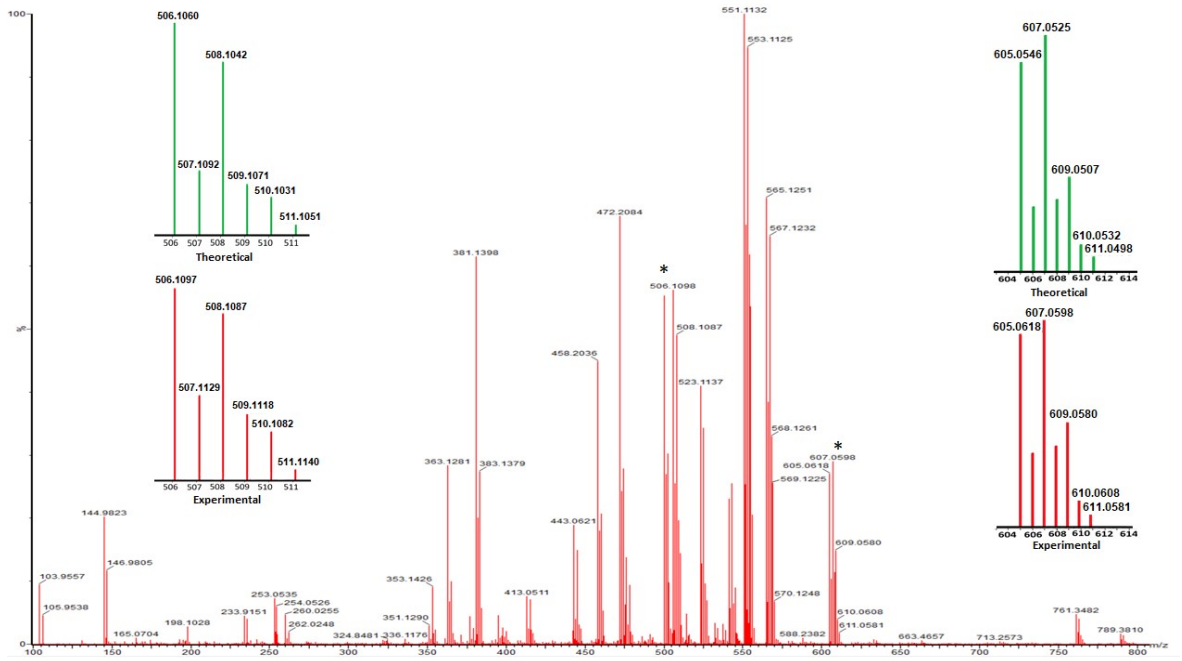

Figure S8. ESI-MS (positive mode) of $[Cu(L_2)]^{2+}$ (**3**) in methanol. Calculated m/z for $[(L_2)Cu]^{+}$: 506.106, Obtained m/z: 506.109; Calculated m/z for $[(L_2)Cu(ClO_4)]^{+}$: 605.054, Obtained m/z: 605.062.

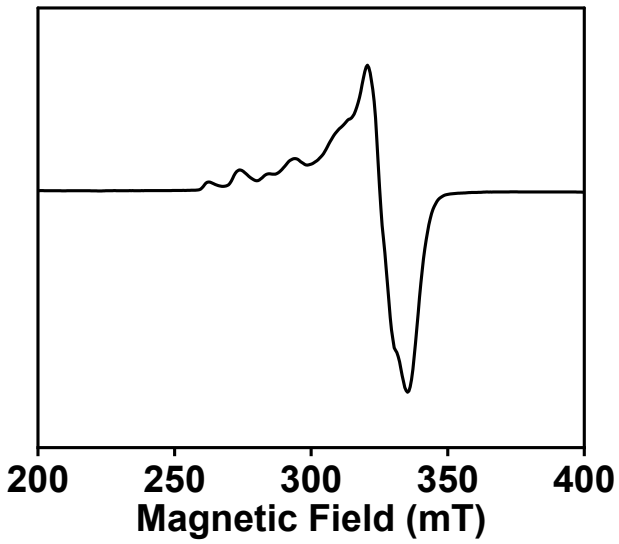

Figure S9. X-band EPR spectrum of **3** (1 mM) in frozen methanol at 77 K.

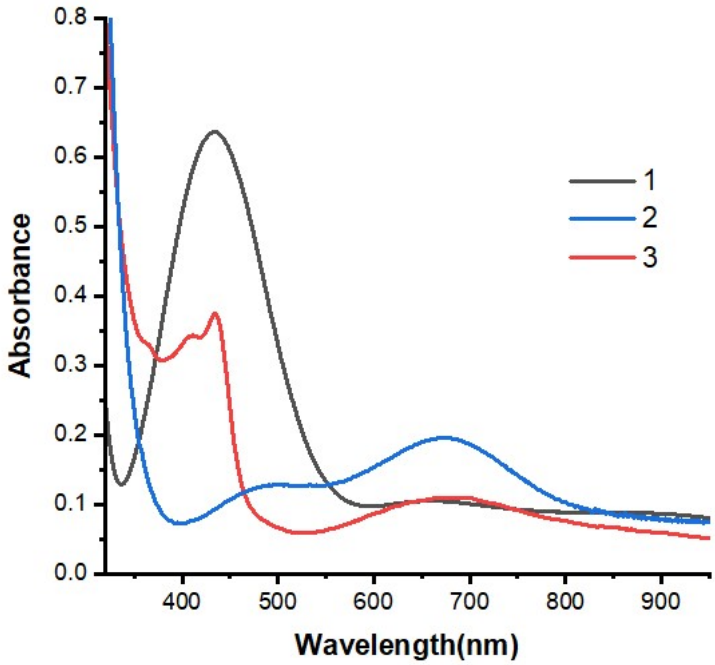

Figure S10. UV-vis spectra of **1** (0.5 mM), **2** (1 mM), and **3** (1 mM) in methanol.

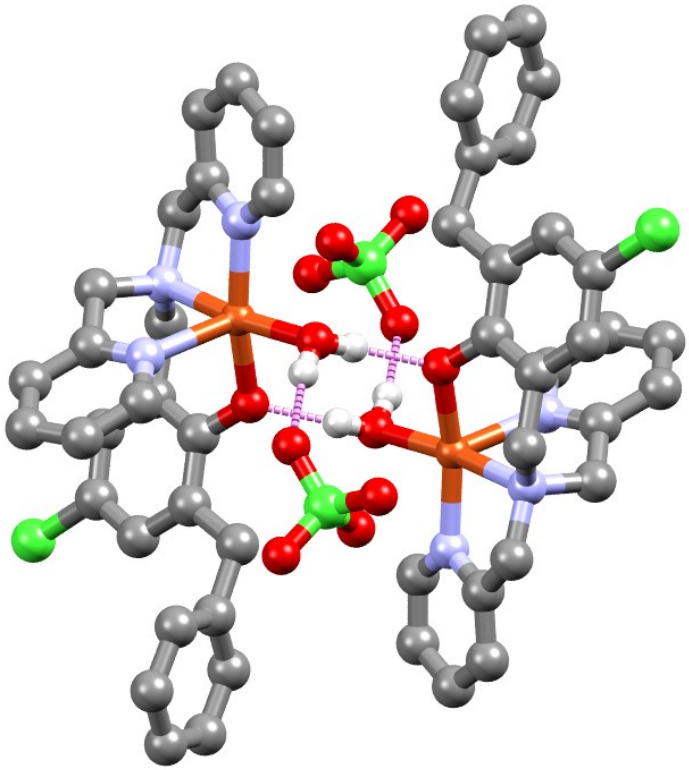

Figure S11. Formation of the supramolecular dimer through hydrogen bonding interaction between two molecules of **1.**

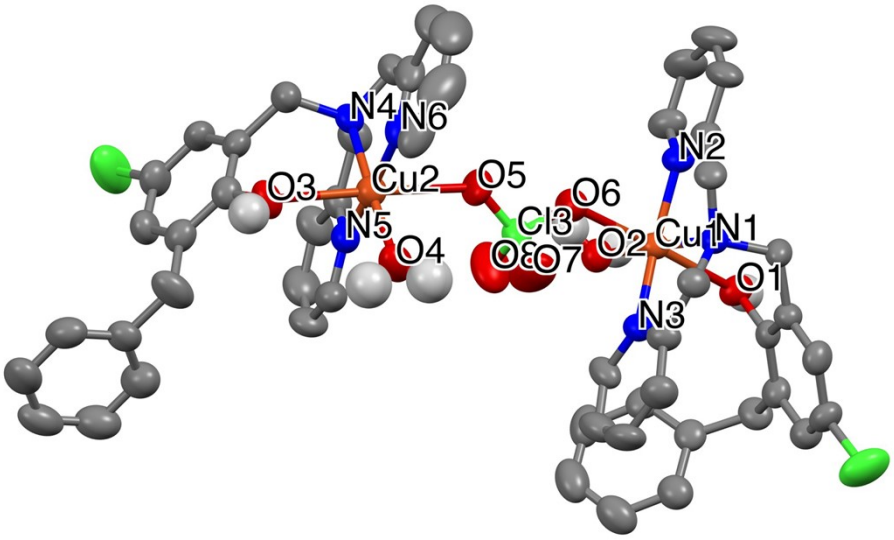

Figure S12. ORTEP diagram of complex **2** with atom labelling scheme in 50 % probability ellipsoids. Uncoordinated perchlorate anions and water molecules are omitted for clarity.

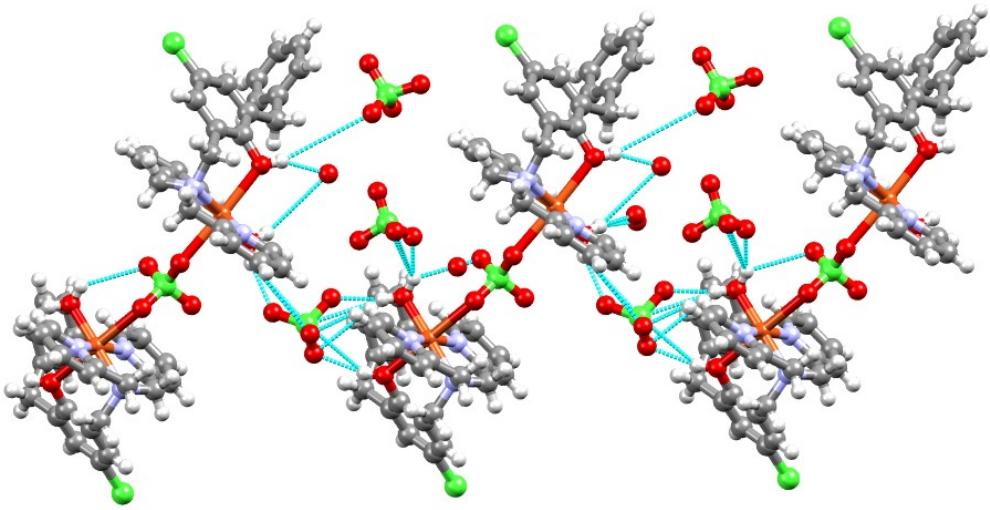

Figure S13. Hydrogen bonding interactions in complex **2**.

Table S4. List of hydrogen bonding interactions for **1** and **2.**

Hydrogen Bonds for 1						
D	**H**	**A**	**d(D-H)/Å**	**d(H-A)/Å**	**d(D-A)/Å**	**D-H-A/°**
O2	H2A	O1[1]	0.84(4)	1.79(4)	2.610(3)	166(3)
O2	H2B	O3[2]	0.835(19)	1.89(2)	2.721(4)	170(4)

[1]2-X,1-Y,1-Z; [2]1+X,+Y,+Z

Hydrogen Bonds for 2						
D	**H**	**A**	**d(D-H)/Å**	**d(H-A)/Å**	**d(D-A)/Å**	**D-H-A/°**
O3	H3A	O21	0.82	1.90	2.676(13)	156.6
O4	H4A	O9	0.85	2.16	2.872(10)	140.9
O4	H4B	O22B	0.85	1.83	2.59(3)	149.7

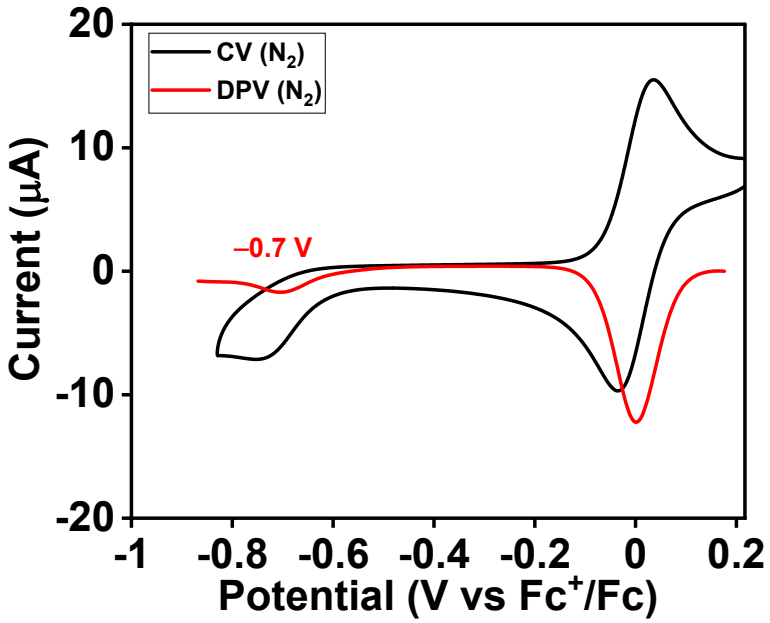

Figure S14. CV and DPV of **1** (0.5 mM) in acetone solution under N_2 atmosphere. Scan rate: 100 mV/s. $^{n}Bu_4PF_6$ (100 mM) was used as the supporting electrolyte.

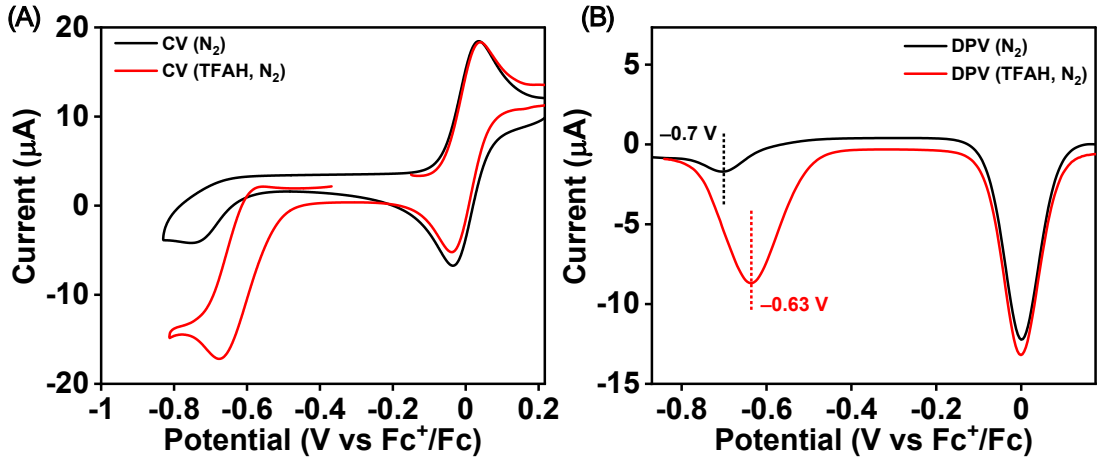

Figure S15. CVs (A) and DPVs (B) of **1** (0.5 mM) in acetone solution under N_2 atmosphere in the presence and absence of TFAH. Ferrocene was added to the solution as an internal standard during the CV/DPV measurements. Scan rate for CV measurements: 100 mV/s. $^{n}Bu_4PF_6$ (100 mM) was used as the supporting electrolyte.

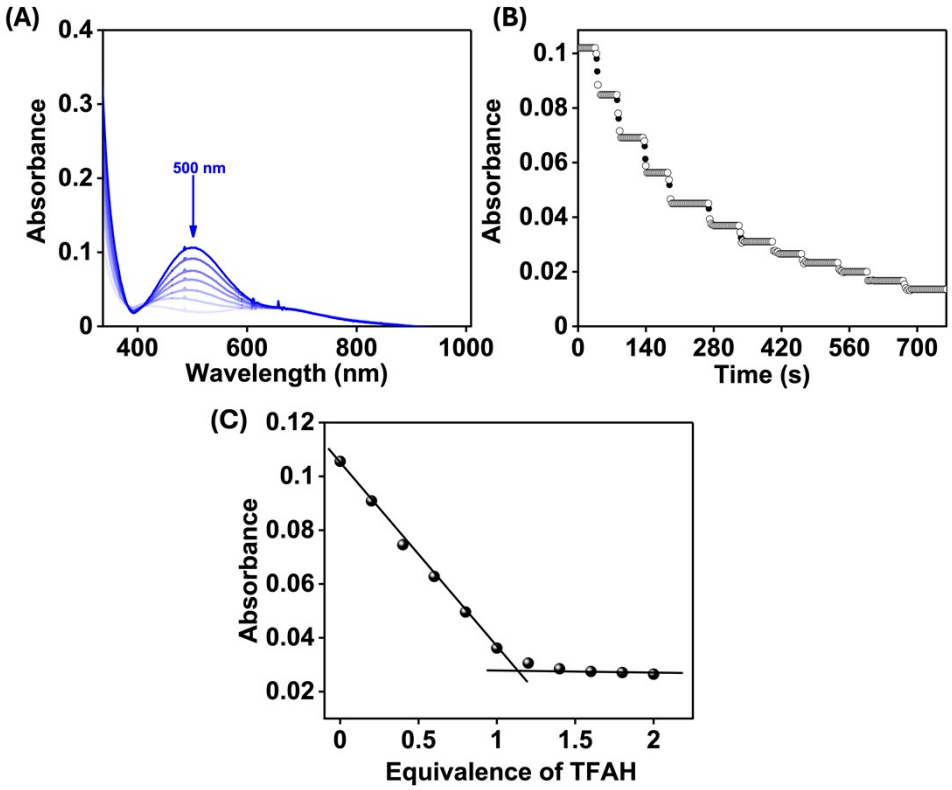

Figure S16. (A) Change of UV-vis spectrum of **1** (0.5 mM) upon incremental addition of TFAH to an acetone solution of the complex, (B) Change of absorbance at 500 nm upon addition of TFAH with time, (C) A plot of Absorbance vs equiv. of TFAH added.

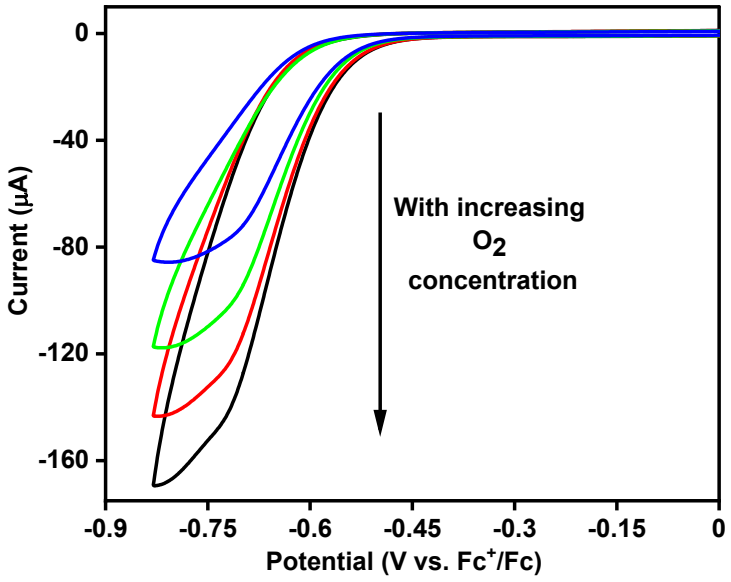

Fig S17. CVs of **1** (0.5 mM) were recorded at different oxygen concentrations in acetone solution containing 10 mM of TFAH. Scan rate = 100 mV/s. $^{n}Bu_4PF_6$ (100 mM) was used as the supporting electrolyte.

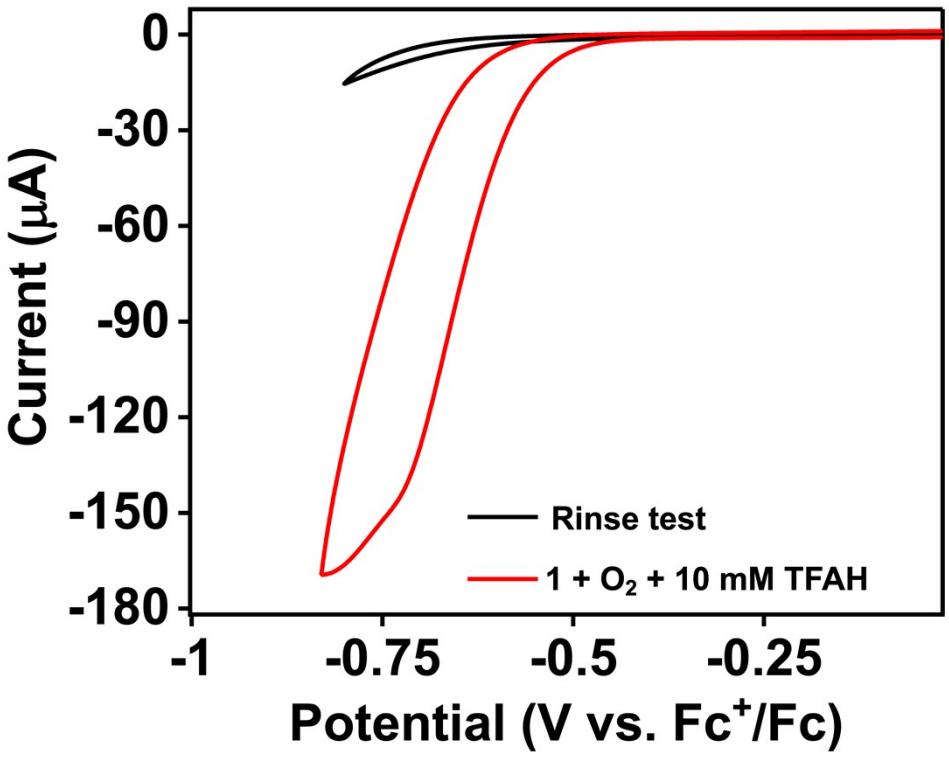

Figure S18. CV data of **1** (0.5 mM) in oxygen-saturated acetone solution containing 10 mM TFAH. The working electrode was then washed with acetone, and CV data were recorded in the fresh acetone solution. Scan rate = 100 mV/s. $^{n}Bu_4PF_6$ (100 mM) was used as the supporting electrolyte.

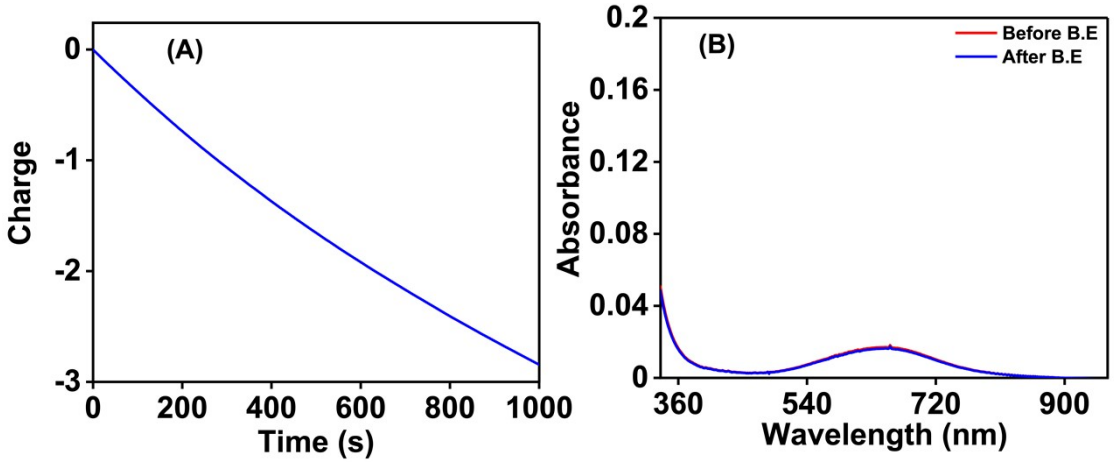

Figure S19. Charge passed in the constant potential electrolysis experiment performed in an oxygen-saturated acetone containing 0.5 mM of **1** and 10 mM of TFAH at an applied potential of −0.8 V vs. Fc^{+}/Fc. $^{n}Bu_4PF_6$ (100 mM) was used as the supporting electrolyte. (B) UV-vis spectrum of the **1** recorded before and after the electrolysis experiment.

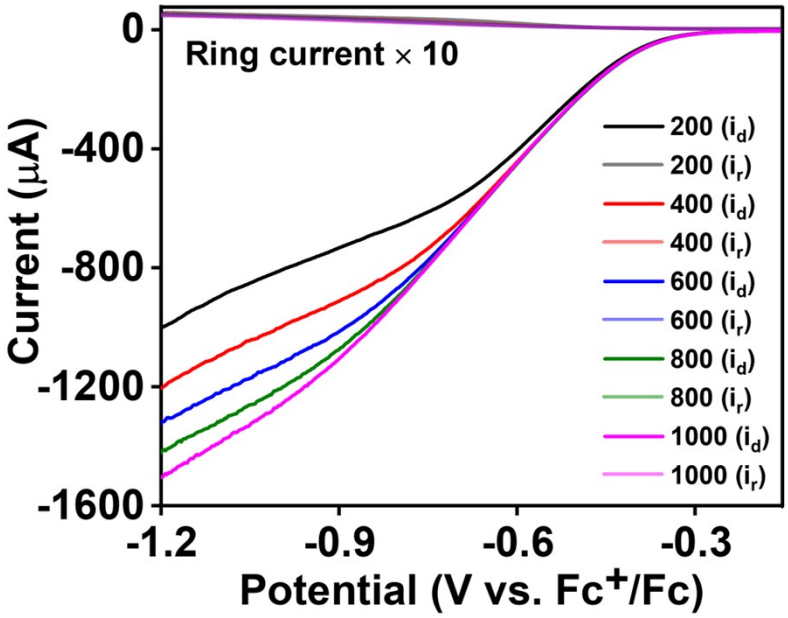

Figure S20. LSV of the RRDE experiments of **1** (0.5 mM) at various rotation rates in the presence of 10 mM of TFAH in an oxygen-saturated acetone solution.

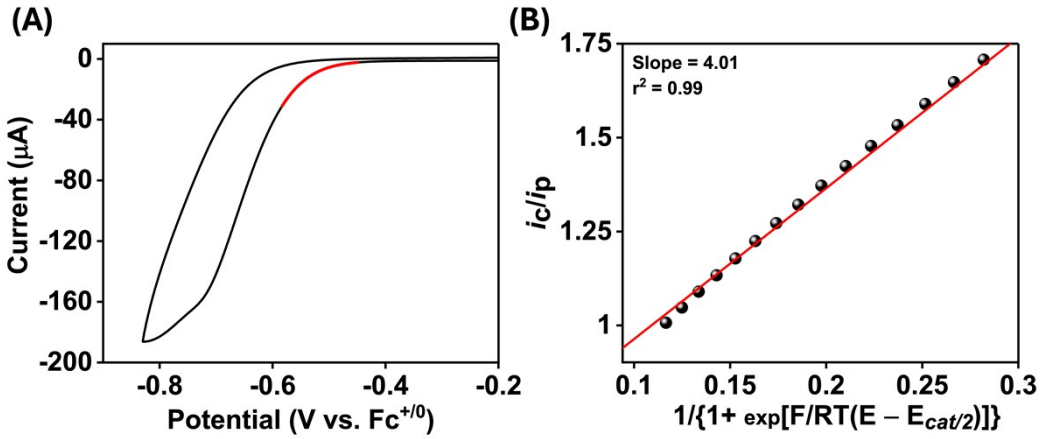

Figure S21. (A) CV data of **1** (0.5 mM) in oxygen-saturated acetone solution containing 10 mM TFAH. Scan rate: 100 mV/s. $^{n}Bu_4PF_6$ (100 mM) was used as the supporting electrolyte. (B) Foot of wave analysis of complex **1**. The red line in the CV diagram indicates the fitted region for FOWA.

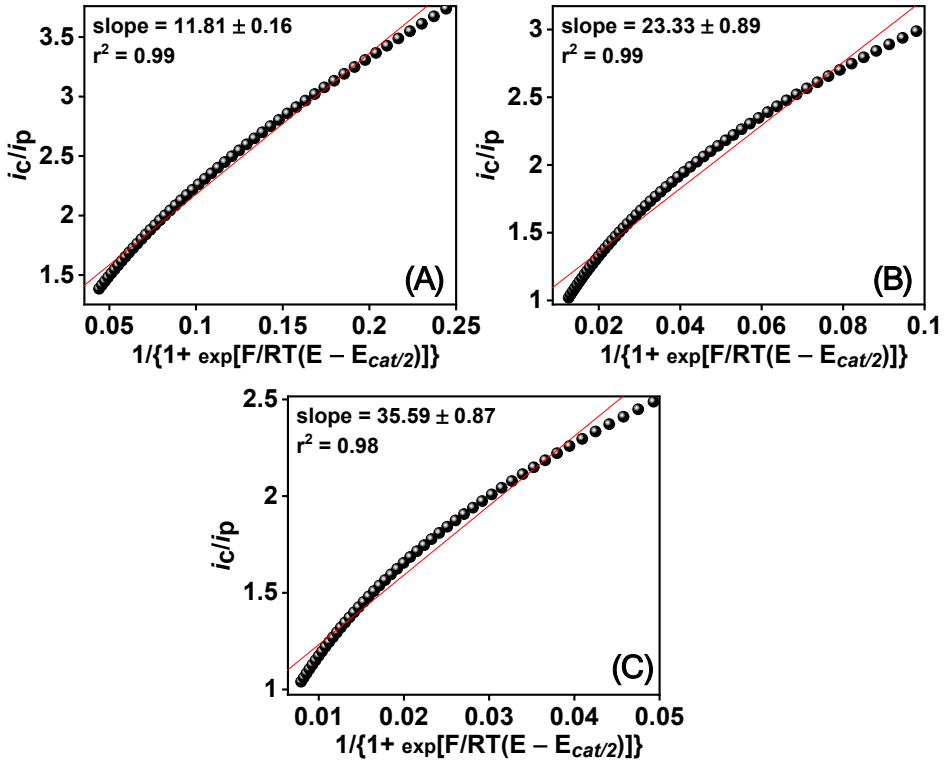

Figure S22. Foot of the wave analysis for the CV data recorded in an oxygen-saturated acetone solution containing complex **1** (0.5 mM) and varying concentrations of TFAH (20 mM (A), 30 mM (B), 40 mM (C)). Scan rate: 100 mV/s.

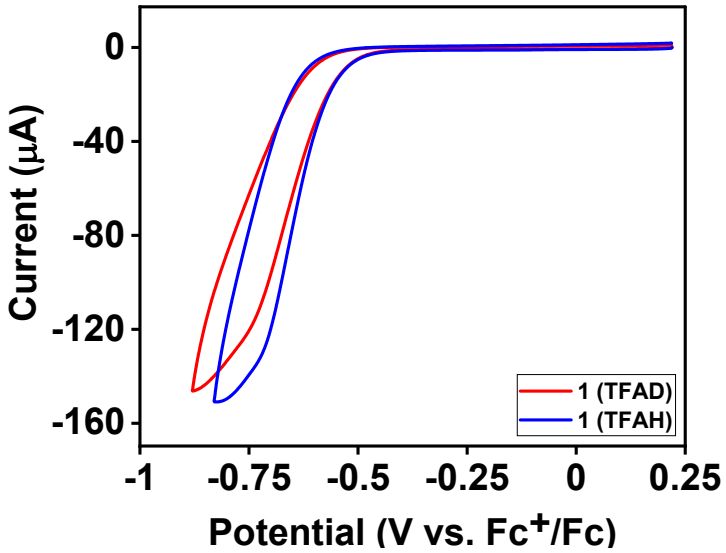

Figure S23. CV of **1** (0.5 mM) at 25 °C in an oxygen-saturated acetone solution in the presence of TFAH (10 mM, blue line) and TFAD (10 mM, red line). $^{n}Bu_4NPF_6$ (100 mM) was used as a supporting electrolyte. A GC working electrode (3 mm), a Pt wire counter electrode, and an Ag/AgCl in saturated KCl as the reference electrode were used during CV measurements. Scan rate: 100 mV/s.

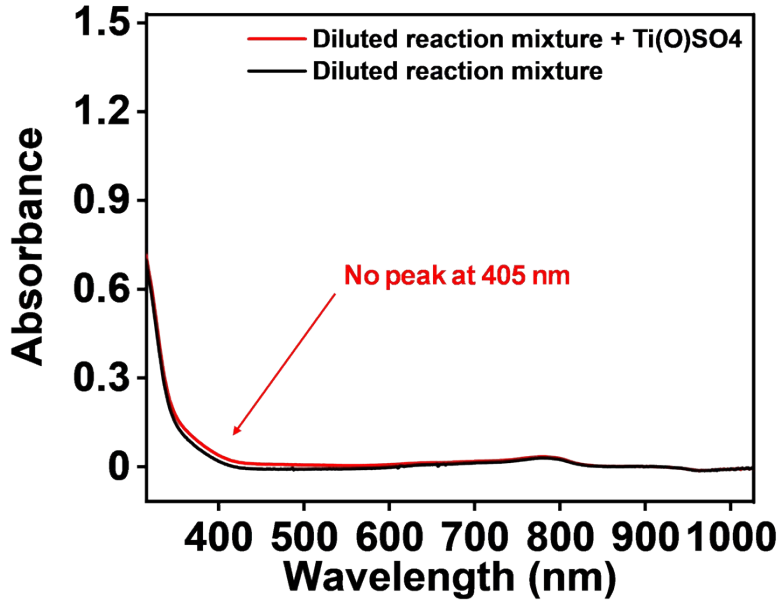

Figure S24. Change of UV-vis spectrum upon addition of 0.1 M $Ti(O)SO_4$ to dilute reaction mixture solution (**1** + TFAH + Fc* + O_2)

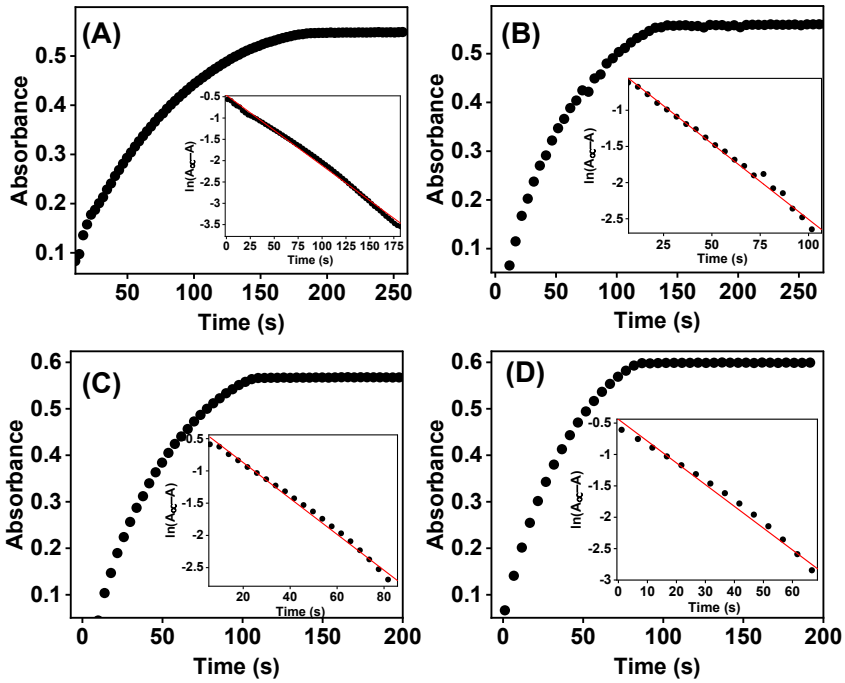

Figure S25. Change of absorbance in the UV-vis spectrum at 780 nm for the reaction of Fc* (1 mM) with O_2 (11 mM) in the presence of 15 mM of TFAH and **1** (0.02 mM (a), 0.03 mM (b), 0.04 mM (c), 0.05 mM (d)). [Inset: Plots of $\ln(A_\infty - A)$ vs time(s) at different concentrations of **1** for the determination of k_{obs} values]

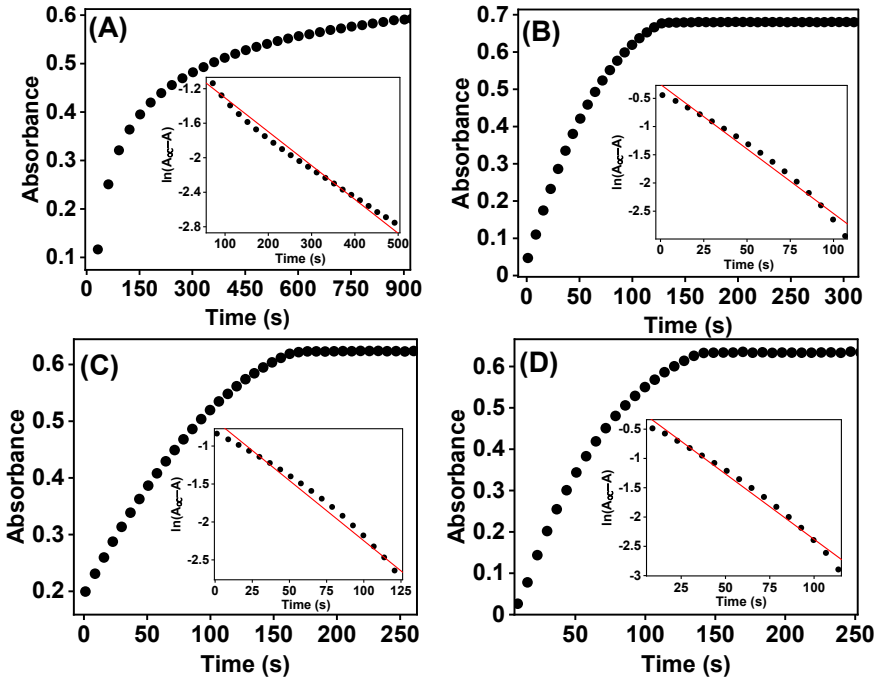

Figure S26. Change of absorbance in the UV-vis spectrum at 780 nm for the reaction of Fc* (1 mM) with O_2 (2 mM (a), 4.5 mM (b), 7 mM (c), 11 mM (d)) in the presence of 15 mM of TFAH and 0.02 mM of **1**. [Inset: Plots of $\ln(A_\infty - A)$ vs time(s) at different concentrations of O_2 for the determination of k_{obs} values]

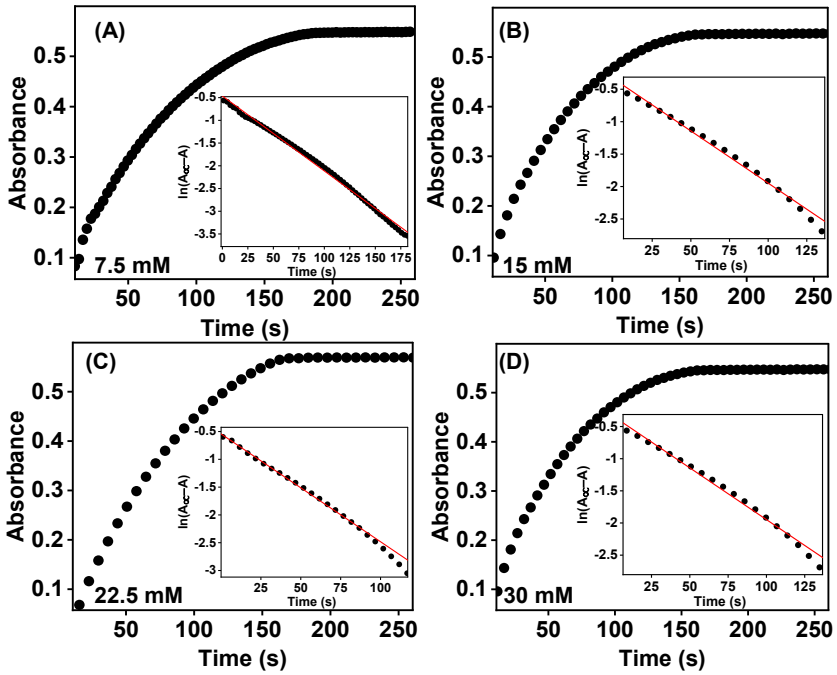

Figure S27. Change of absorbance in the UV-vis spectrum at 780 nm for the reaction of Fc* (1 mM) with O_2 (11 mM) in the presence of 0.02 mM of **1** and TFAH (7.5 mM (a), 15 mM (b), 22.5 mM (c), 30 mM (d)). [Inset: Plots of $\ln(A_\infty - A)$ vs. time(s) at different concentrations of TFAH for the determination of k_{obs} values]

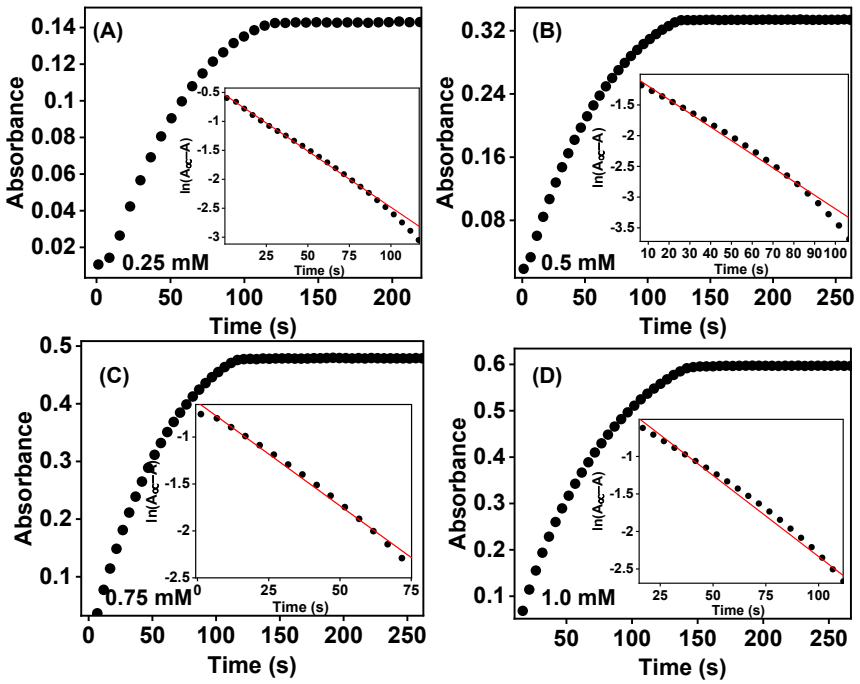

Figure S28. Change of absorbance in the UV-vis spectrum at 780 nm for the reaction of Fc* (0.25 mM (a), 0.5 mM (b), 0.75 mM (c), 1 mM (d)) with O_2 (11 mM) in the presence of 10 mM of TFAH and 0.02 mM of **1**. [Inset: Plots of $\ln(A_\infty - A)$ vs time (s) at different concentrations of Fc* for the determination of k_{obs} values]

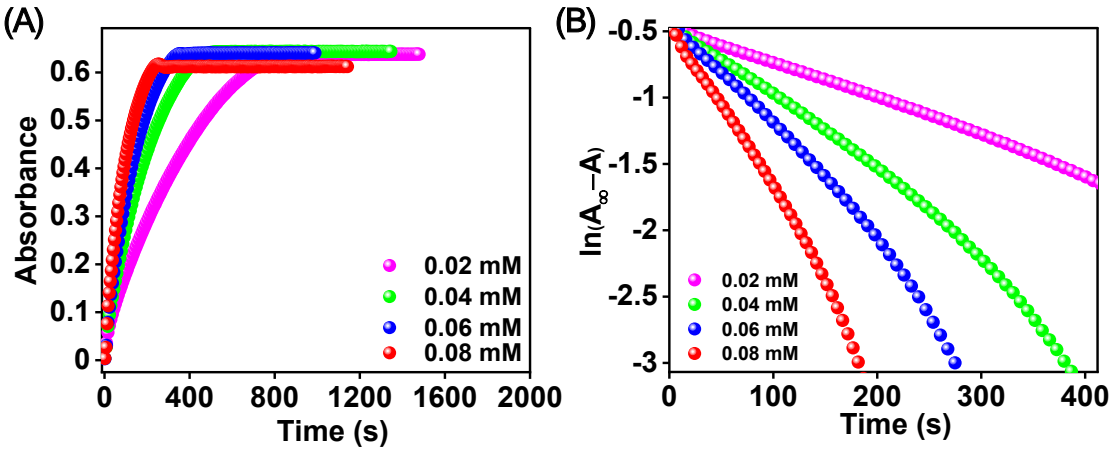

Figure S29. (A) Change of absorbance in the UV-vis spectrum at 780 nm for the reaction of Fc* (1 mM) with O_2 (11 mM) in the presence of 15 mM of TFAH and **3** (0.02 mM, 0.03 mM, 0.04 mM, 0.05 mM). (B) Plots of $\ln(A_\infty - A)$ vs time (s) at different concentrations of **3** for the determination of k_{obs} values.

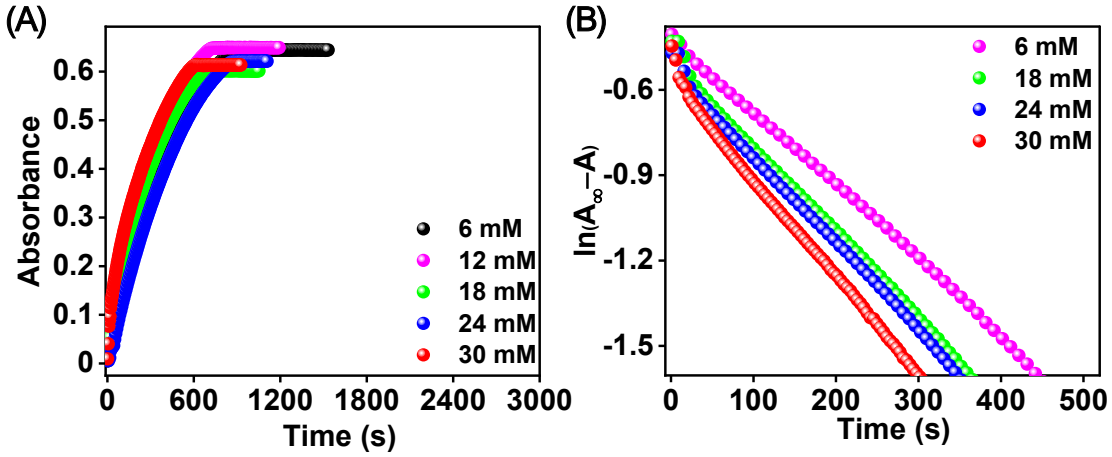

Figure S30. (A) Change of absorbance in the UV-vis spectrum at 780 nm for the reaction of Fc* (1 mM) with O_2 (11 mM) in the presence of 0.02 mM of **3** and TFAH (6 mM, 18 mM, 24 mM, 30 mM). (B) Plots of $\ln(A_\infty - A)$ vs. time (s) at different concentrations of TFAH for the determination of k_{obs} values.

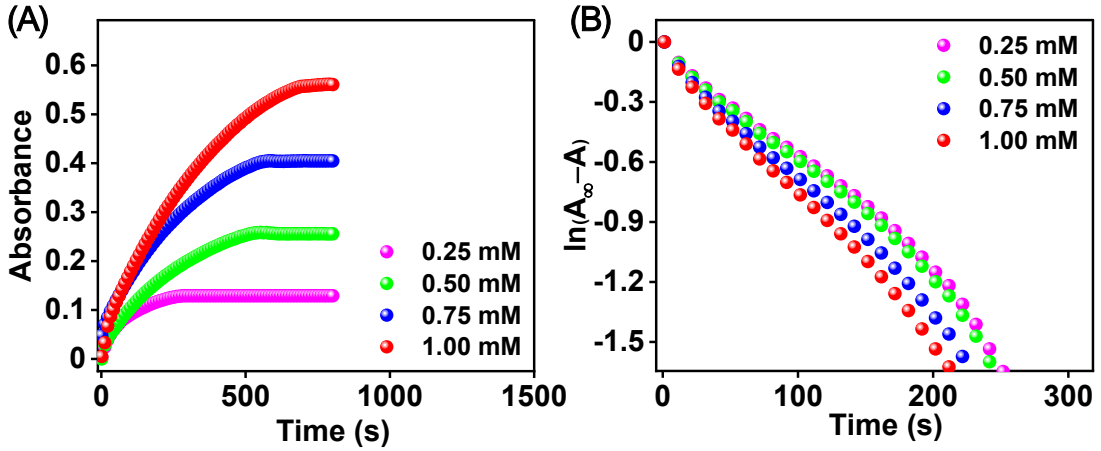

Figure S31. (A) Change of absorbance in the UV-vis spectrum at 780 nm for the reaction of Fc* (0.25 mM, 0.5 mM, 0.75 mM, 1 mM) with O_2 (11 mM) in the presence of 10 mM of TFAH and 0.02 mM of **3**. (B) Plots of $\ln(A_\infty - A)$ vs time (s) at different concentrations of Fc* for the determination of k_{obs} values.

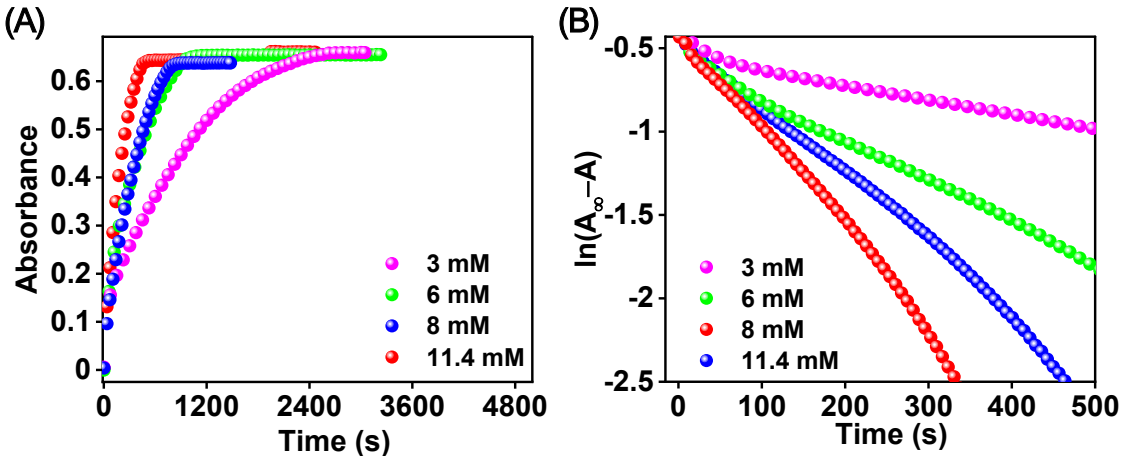

Figure S32. (A) Change of absorbance in the UV-vis spectrum at 780 nm for the reaction of Fc* (1 mM) with O_2 (3 mM, 6 mM, 8 mM, 11.4 mM) in the presence of 15 mM of TFAH and 0.02 mM of **3**. (B) Plots of $\ln(A_\infty - A)$ vs time (s) at different concentrations of O_2 for the determination of k_{obs} values.

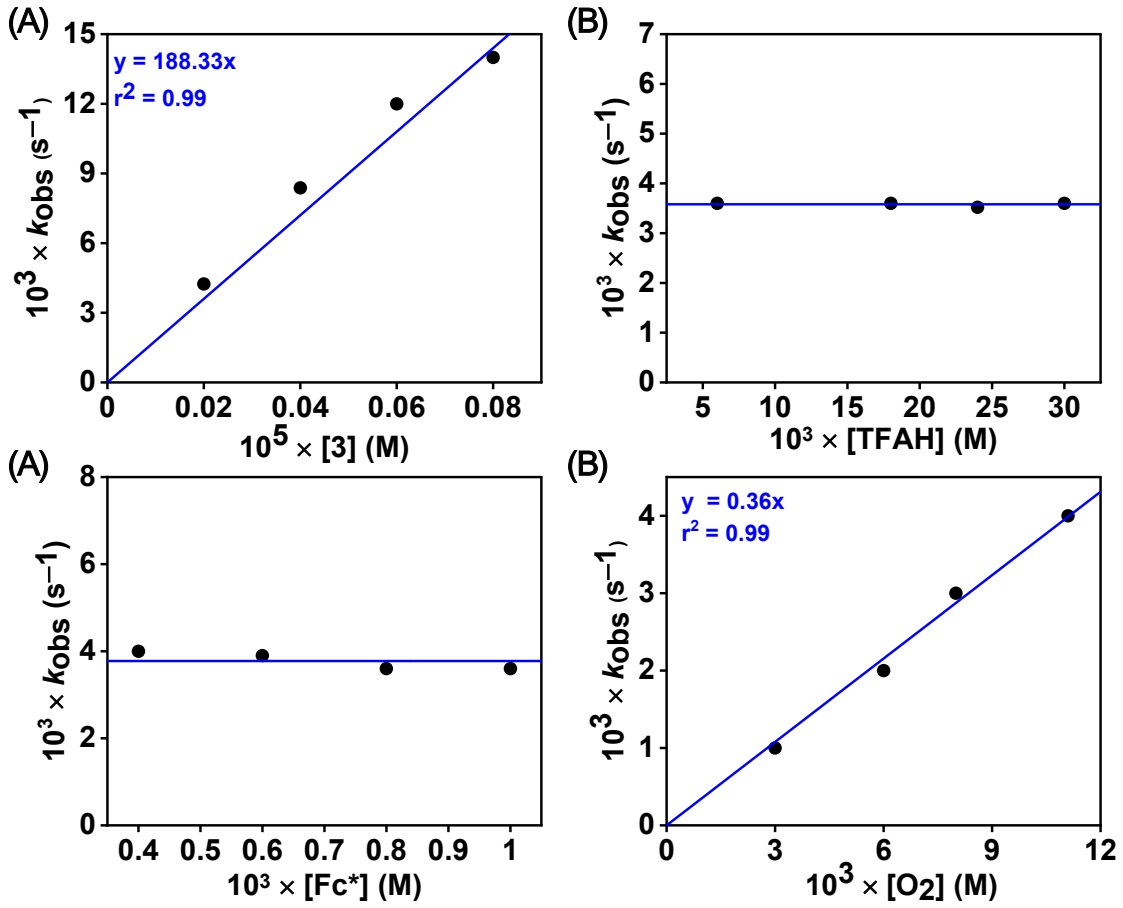

Figure S33. Plot of the pseudo-first-order rate constant (k_{obs}, s^{-1}) vs. concentration (M) of different substrates: (A) k_{obs} vs. [**3**]; (B) k_{obs} vs. [TFAH]; (C) k_{obs} vs. [Fc*]; and (D) k_{obs} vs. [O_2].

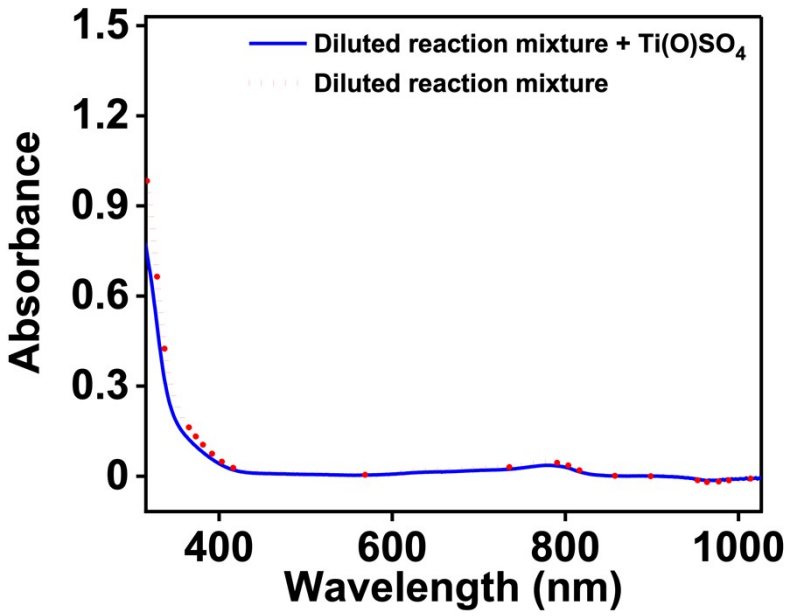

Figure S34. Change of UV-vis spectrum of the reaction solution obtained upon addition of 0.1 M $Ti(O)SO_4$ to the dilute reaction mixture (**3** + TFAH + Fc* + O_2).

References

[1] D. Mondal and M. C. Majee, *Inorganica Chim. Acta*, 2017, **465**, 70–77.

[2] D. D. Perrin, W. L. F. Armarego and D. R. Perrin, Purification of Laboratory Chemicals, 2nd ed.; *Pergamon: Oxford, U.K.,* 1980**.**

[3] SADABS (version 2.03), Program for Empirical Absorption Correction of Area Detector Data; Bruker AXS Inc.: Madison, WI, 2002.

[4] G. M. Sheldrick, *Sect. A: Found. Crystallogr.* 1990, **46**, 467−473.

[5] (a) Sheldrick, G. M. SHELXL−2013, Program for Crystal Structure Refinements; University of Göttingen: Göttingen: Germany, 2013. (b) O. V. Dolomanov, L. J. Bourhis, R. J. Gildea, J. A. K. Howard and H. Puschmann, *J. Appl. Crystallogr.* 2009, **42**, 339−341.

[6] SAINT-plus, Software Users' Guide, version 6.02; Bruker Analytical X-ray Systems Inc.: Madison, WI, 2002.